Atomic kinetics of matter irradiated by intense laser fields

Yechiel Frank,[1,2,*] Arie Zigler,[1] and Zohar Henis[1,2]
[1]*Racah Institute of Physics, Hebrew University, Jerusalem 91904, Israel*
[2]*Soreq Research Center, Yavne 81800, Israel*
(Received 5 November 2015; published 27 September 2016)

The atomic kinetics of solid density low-Z material under an intense oscillating laser field is presented. The transient behavior of the average ionization and the heating mechanism is analyzed. Temporal oscillations in excited configurations populations caused by the laser field oscillations are demonstrated. These phenomena present a method for creating short, 1–100 fs, monochromatic but incoherent x-ray pulses and for measuring basic atomic rates.

DOI: 10.1103/PhysRevE.94.033209

I. INTRODUCTION

The understanding of the interaction of short $\tau < 1$ ps, intense $I > 10^{15}\mathrm{W/cm}^2$ laser pulses with matter has been the focus of many works in the past, both experimentally and theoretically [1–3]. Many of these studies have been motivated by a desire to generate photons and particles with energies far above the energy of a single laser photon. In particular, some of these experiments have investigated the production of incoherent and coherent x-ray radiation. These experiments were performed using two types of targets, gas targets, and solid targets. In gas targets, much progress has been made in the generation of bright, coherent soft x rays in the 30–100 eV range through harmonic generation and x-ray lasers [4,5]. Typically, these experiments involve focusing the short laser pulse into a static filled gas cell or at the output of a pulsed gas jet. Gas phase targets are attractive for use in x-ray generation with short pulse lasers for a number of reasons. Since the laser propagates through the medium, coherent x-ray generation is possible through harmonic generation, or through the creation of a plasma channel suitable for x-ray laser gain. Furthermore, gas targets generate no debris. Gases, however, usually exhibit poor absorption of laser energy and are, therefore, limited in their effective convergence of laser light into x rays. Solid targets, on the other hand, often exhibit larger laser energy absorption. The use of solids as targets for intense lasers has successfully produced both photons and particles with energies in the MeV range [6–8]. In many experiments, measurements and theoretical analysis are performed on time scales of the laser pulse. The underlying assumption was that the system is static within a single laser cycle duration. Hence, the calculations are performed using cycle-averaged values and measurements are done at time scales $\geqslant$100 fs.

The present work presents a possible method for creating fs time scale x-ray pulses. The duration of the x-ray radiation is a key parameter for its application to the analysis of rapidly evolving phenomena. For example, such sources can be used to complement optical lasers femtochemistry [9]. Another example is the investigation of molecular structure without the need for crystallization. This will give access to biomolecules yet impossible to crystallize.

The focus of the present work is to investigate the atomic kinetics of solid density targets under an intense fs laser pulse. The simulations are performed time dependently without cycle averaging. Two characteristic time scales are identified. First, a longer time scale (10–100 fs) on which the heating and collisional ionization of the target take place. Second, we show that at high densities both collisional atomic processes rates and laser field induced ionization rates are much larger than the laser frequency. The temporal population distribution of the various excited atomic states is therefore determined by the instantaneous ratio between these rates and not their average value. These results create new possibilities for short x-ray sources and for experimentally measuring collisional excitation rates in plasmas.

This paper is organized as follows. In Sec. II the simulation method is described. The calculation of the internal and laser-induced atomic rates are described. The calculation of the heating rate is also derived. In Sec. III the time evolution of the electron temperature and average ionization for a carbon target is presented and analyzed. Section IV shows the temporal population of the various configurations. The kinetic processes resulting in this temporal behavior are explained. Section V demonstrates the role of the averaged vs nonaveraged laser ionization rate on the temporal shape of x-ray emission from the target. In Sec. VI we explain how the same kinetic description leads to different emission patterns at different laser intensities. Section VII we demonstrate the effect for different target materials. The influence of higher-density and higher-Z material are further analyzed. Finally, we conclude our findings and give some basic layout for possible experimental ways of measuring these effects in Sec. VIII.

II. ATOMIC SIMULATION

In order to make quantitative predictions about the nature of intense laser pulse interactions with materials we require a model that accounts for the various processes that occur within the time scale of the laser pulse. Moreover, for solid density targets many of the atomic processes occur on time scales shorter than the laser oscillation time ($2\pi/\omega_l$). These will include laser energy absorption, ionization, recombination, excitation, and deexcitation processes. In all calculations presented in this work a short pulse time (100 fs) was used leading to negligible hydrodynamic expansion of the target [10,11]. We focus on describing the kinetic behavior within the laser

*yechiel.frank@mail.huji.ac.il

penetration layer, skin depth. We shall therefore assume that the density within the target skin depth is uniform and unchanged throughout the laser interaction.

We shall assume that the collisionality inside the target skin depth is high enough and its size is small enough that no thermal gradients exist within the laser penetration skin depth. Thus, we can assume that the temperature is uniform and the electron velocity distribution is isotropic and can be described by a Maxwellian. This assumption is valid when the electron thermalization time is smaller than the laser oscillation time. The electron-electron collisions frequency in a plasma is given by [12]:

$$\nu_{ee} \approx 5.8 \times 10^{-6} T^{-3/2} n_e \Lambda_{ee}, \tag{1}$$

where T is the electron temperature (all temperatures are in eV), n_e the electron density, and Λ_{ee} is the Coulomb logarithm. For solid density plasmas, at the temperature range of 1–700 eV, the values of the electron-electron collisions obtained from Eq. (1) are $10^{16} \rightarrow 10^{18}$ s^{-1}. The laser field oscillations frequency is only $\approx 10^{15}$ s^{-1}.

In order to calculate the heating of the target skin layer, we follow Ref. [13]. The wave equation of the electric field inside a solid target for a linearly polarized monochromatic wave with frequency ω at normal incident along the z axis is

$$\frac{\partial^2 E(z)}{\partial z^2} + \frac{\epsilon(\omega,z)\omega^2 E(z)}{c^2} = 0. \tag{2}$$

This equation is known as the Helmholtz equation [14]. $\epsilon(\omega,z)$ is the dielectric permittivity of the target. For a constant ϵ and a vanishing electric field at infinity, the solution of Eq. (2) is

$$E(z) = E(0) \exp\left(-\frac{z}{\delta}\right). \tag{3}$$

$E(z)$ is the spatial form of the electric field transmitted into the solid target. Substituting the solution of Eq. (3) into Eq. (2) yields a skin depth δ of:

$$\delta = \frac{ic}{\sqrt{\epsilon}\omega}. \tag{4}$$

We use a simple Drude model for the plasma dielectric constant:

$$\epsilon = 1 - \frac{\omega_p^2}{\omega(\omega + i\nu)}, \tag{5}$$

where $\omega_p = (4\pi q^2 n_e/m_e)^{1/2}$ is the plasma frequency, $\nu \approx 10^{-5} n_e T_e^{-3/2}$ [15] is the electron-ion collision frequency. Substituting Eq. (5) into Eq. (4) one gets:

$$\begin{aligned}\delta &= \frac{c}{\omega_p}\left(\frac{1 + i(\nu/\omega)}{1 - (\omega^2/\omega_p^2) - i(\nu\omega/\omega_p^2)}\right)^{1/2} \\ &\approx \frac{c}{\omega_p}\left(1 + i\frac{\nu}{\omega}\right)^{1/2} for\ \omega_p \gg \omega.\end{aligned} \tag{6}$$

In the case of solid targets $\omega_p \approx 2 \times 10^{16} \gg \omega$ and therefore the last approximation is valid. The skin depth is therefore given by:

$$\delta = \begin{cases} \frac{c}{\omega_p} & \text{for } \frac{\nu}{\omega} \ll 1 \text{ and } \frac{\omega}{\omega_p} \ll 1 \\ \frac{c}{\omega_p}\left(\frac{\nu}{2\omega}\right)^{1/2} & \text{for } \frac{\nu}{\omega} \gg 1 \text{ and } \frac{\omega}{\omega_p} \ll 1. \end{cases} \tag{7}$$

The laser reflection coefficient, R and absorption coefficient A are given by [16]:

$$R = \left\| \frac{1 - \sqrt{\epsilon}}{1 + \sqrt{\epsilon}} \right\|^2 \quad A = 1 - R. \tag{8}$$

Using the dielecric coefficient of Eq. (5) for the absorption coefficient one gets:

$$A = \begin{cases} \frac{2\nu}{\omega_p} & \text{for } \frac{\nu}{\omega} \ll 1 \text{ and } \frac{\omega}{\omega_p} \ll 1 \\ \frac{2\nu}{\omega_p}\sqrt{\frac{\omega}{\nu}} & \text{for } \frac{\nu}{\omega} \gg 1 \text{ and } \frac{\omega}{\omega_p} \ll 1. \end{cases} \tag{9}$$

The heating rate per unit volume in the laser skin depth is therefore

$$\frac{\partial U}{\partial t} = \frac{AI(t)}{\delta}, \tag{10}$$

where U is the energy density per unit volume, A is the absorption coefficient given by Eq. (9), $I(t)$ is the time-dependent intensity of the specific laser pulse, and δ is the laser penetration skin depth given by Eq. (7). We then assume simple ideal gas distribution of the absorbed energy among the free electrons given by:

$$U = \frac{3}{2} N K_b T, \tag{11}$$

where N is the number of particles per unit volume and K_b is the Boltzmann constant.

In the present work, the laser field propagation into the target is not modeled. The Helmholtz equation (Eq. (2)) is not numerically solved. We focus on a zero-dimensional simulation of the laser skin depth layer where the field intensity can be viewed as approximately unchanged. The laser field only decreases by a factor of $(1/e)$ according to Eq. (3) within the skin depth.

For this layer we solve the atomic kinetics together with the thermal evolution, according to Eq. (10), to obtain the spectral behavior of the plasma. For the atomic kinetics we follow a detailed configuration accounting (DCA) approach for nonrelativistic configurations (NRC). All rates, cross sections, and level energies for singly excited configurations are calculated using the HULLAC code [17]. In order to include multiply excited configurations we use the SEMILLAC model extension method as described in Refs. [18,19].

Each ionic nonrelativistic configuration (NRC) is described by the occupation numbers w_i in electron subshell $n_i l_i$

$$c \equiv n_1 l_1^{w_1} \ldots n_i l_i^{w_i} \ldots n_K l_K^{w_K}. \tag{12}$$

Our model considers average atomic quantities for these NRCs. The energy averaging is performed according to:

$$E_c = \frac{\sum_{i \in c} g_i E_i}{\sum_{i \in c} g_i}, \tag{13}$$

where E_c is the statistically weighted averaged energy of the NRC, E_i is the energy of a single level within the NRC, and g_i is the statistical weight of that level. We set the ground NRC average energy of the ion to have $E_{g.s\ NRC} = 0$ and shift all the ionic NRCs averaged energies accordingly. The ionization potential of each ionic stage is calculated using HULLAC and corrected, to account for the pressure ionization-continuum lowering effect using Stewart and Pyatt model [20].

In a similar fashion, the averaged transition rate, radiative or collisional from one NRC to another NRC is averaged according to:

$$R_{c\to c'} = \frac{\sum_{i\in c, j\in c'} g_i R_{i\to j}}{\sum_{i\in c} g_i}, \tag{14}$$

$R_{i\to j}$ being the rate coefficient of transition from any level i included in the initial NRC of the transition, c, to any level j included in the final NRC, c'. The average is weighted according to g_i, the statistical weight of the initial level of the transition.

The atomic processes included in the collisional radiative model (CRM) are

(i) radiative decay,
(ii) collisional excitation,
(iii) collisional deexcitation,
(iv) collisional ionization,
(v) three-body recombination,
(vi) radiative recombination,
(vii) autoionization,
(viii) electron capture,
(ix) laser-induced ionization.

The laser-induced ionization rate is given by the static field tunnel ionization formula of Landau [21]:

$$R_{\text{laser}}(t) = 4\omega_0 \left(\frac{E_i}{E_h}\right)^{5/2} \frac{E_a}{E(t)} \exp\left[-\frac{2}{3}\left(\frac{E_i}{E_h}\right)^{3/2} \frac{E_a}{E(t)}\right], \tag{15}$$

where $\omega_0 = me^4/\hbar^3$ is the atomic frequency unit, E_h and E_i are the ionization potentials of hydrogen and of the ionic configuration in question respectively and $E_a = m^2e^5/\hbar^4$ is the atomic unit of the electric field. The use of the static tunneling approximation is justified when the interaction is in the low-frequency–high-intensity regime. as defined by the Keldish parameter [22]

$$\gamma = \frac{\omega_{\text{laser}}}{\omega_{\text{tunneling}}} = \frac{\omega_l (2m_e E_i)^{1/2}}{eE(t)}. \tag{16}$$

Here $\omega_{\text{laser}} = \omega_l$ is the laser frequency and $\omega_{\text{tunneling}}$ is the tunneling ionization rate. When $\gamma \ll 1$ the dominant ionization mechanism is tunneling ionization. All cases studied in the present work are within this regime.

The model consists of a set of coupled rate equations, each describing the population density of a single nonrelativistic configuration,

$$\frac{dN_{\xi m}}{dt} = \sum_{\xi' m'} N_{\xi' m'} \times R_{\xi' m'\to \xi m} - \sum_{\xi' m'} N_{\xi m} \times R_{\xi m\to \xi' m'}, \tag{17}$$

where $N_{\xi m}$ is the density number of ion ξ in configuration m, $R_{\xi' m'\to \xi m}$ is the total rate coefficient populating the ξm configuration from $\xi' m'$, and $R_{\xi m\to \xi' m'}$ is the total depopulating rate coefficient from ξm to any $\xi' m'$ configuration for all the considered atomic processes described above.

This set of equations [Eq. (17) and Eq. (10)] is then solved time dependently, in the presence of the laser pulse and after the pulse ends. The temperature calculated using Eqs. (10) and (11), is used to calculate the atomic rates in Eq. (17) and the total electron density calculate by Eq. (17) is used to calculate the energy distribution in Eqs. (10) and (11).

III. TEMPERATURE AND IONIZATION EVOLUTION

Let us now consider the case of a solid density, carbon target irradiated by an ultraintense fs Ti:sapphire laser pulse, with a wavelength of $\lambda = 0.8\,\mu$m. The laser pulse time is taken to be: $\tau_l = 100$ fs and we use top-hat laser temporal shape for simplicity. The laser intensity is taken to be $I = 2\times 10^{16}\text{W/cm}^2$. The intensity within the skin depth therefore varies from $2\times 10^{16}\text{W/cm}^2$ to $0.73\times 10^{16}\text{W/cm}^2$. The calculations hereafter are performed at an intermediate intensity of $1\times 10^{16}\text{W/cm}^2$. The target is initially at a density of 0.9g/cm^3.

Figure 1 shows the time evolution of the electron temperature and average ionization in the target.

The ionization dynamics can be characterized by three stages. The first stage happens instantaneously. At such laser intensity the target instantly heats up to an electron temperature of 20–30 eV. At such conditions, the first two outer $2p$ electrons are pressure ionized. One can also view this as the target initial conditions. At a second stage additional two electrons are quickly ionized from the $2s$ shell, by the laser field. The ionization potentials of these electrons after consideration of the continuum lowering effect are 9 and 15 eV respectively. This high ionization rate is in agreement with the threshold intensity given in Ref. [23] for the cycle averaged case. The ionization potential of the next ionization stage, He-like, is 330 eV. Therefore, the ground configuration of the He-like ions can not be field ionized by a laser at intensity of $I = 10^{16}\text{W/cm}^2$. At the third stage the atomic kinetics in the target is dominated by collisional processes of ionization and excitation. Laser-induced ionization can take place at this stage as a two-step process. Collisional excitation from the ground state to an excited configuration with a much lower ionization energy. The excited configuration can then be ionized by the laser field. During this third stage the target continues to heat up, to a final temperature of 640 eV. This final temperature

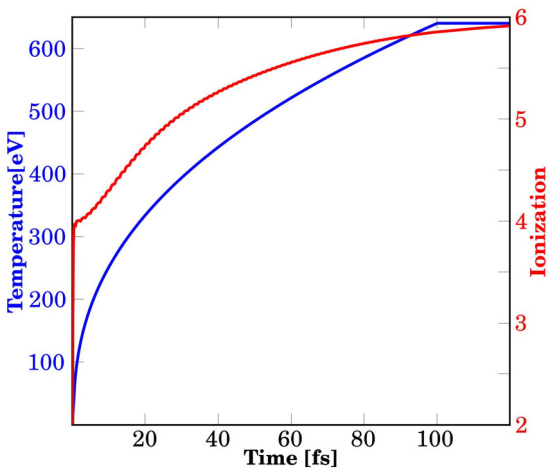

FIG. 1. Time evolution of the electron temperature curve (bottom, blue), and average ionization in the target curve (top, red).

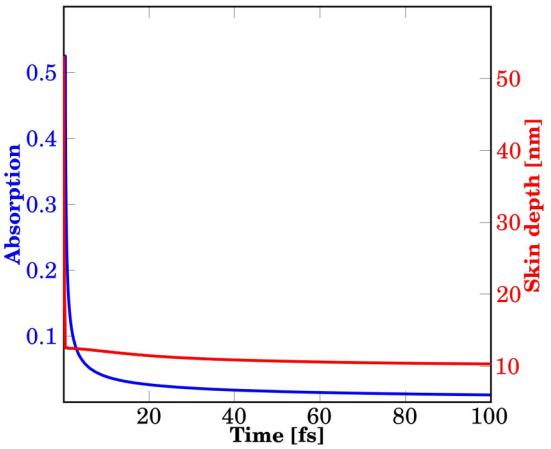

FIG. 2. Time-dependent skin depth top curve (red) and absorption coefficient bottom curve (blue).

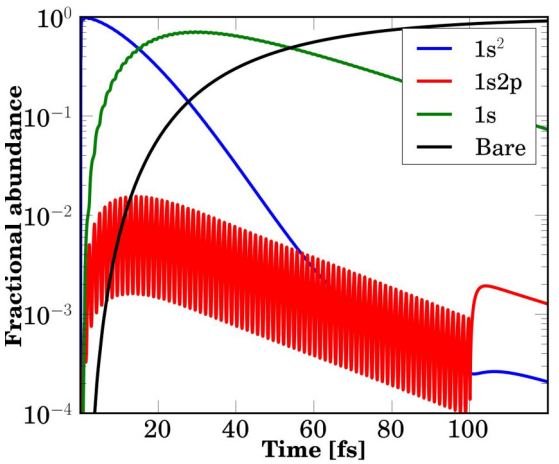

FIG. 3. Time evolution of the fractional populations of four most populated configurations.

is in agreement with temperature values obtained in previous works [10]. Eventually, the average ionization reaches close to fully stripped stage $\bar{Z} = 5.9$. This ionization stage is equal to the steady-state ionization stage of carbon plasma at the same conditions.

Figure 2 shows the time-dependent skin depth and absorption coefficient of the carbon target.

The values for the skin depth and absorption coefficient are calculated according to Eq. (7) and Eq. (9) respectively. These values are then used in Eq. (10) to obtain the target heating rate. Both values are approximately constant through most of the laser pulse duration.

IV. POPULATION DISTRIBUTION

Let us now focus on the population of four specific configurations: ground-state He-like ion $1s^2$, excited-state He-like ion $1s2p$, ground-state H-like ion $1s$, and the fully striped ion. The atomic model includes many other configurations, the total number of configurations is calculated according to the continuum lowering limit. However, these four configurations are the most populated throughout the pulse duration.

Figure 3 shows the time evolution of the fractional populations for these four configurations. As described in Sec. III, the $1s^2$ becomes the most populated configuration in the plasma, shortly after the beginning of the pulse. It then gets depopulated due to the collisional ionization. Then, ground configurations of the H-like and bare ions get populated until almost all bound electrons are stripped. The excited configuration $1s2p$, gets to a maximum population of $\approx$1% only. It is then depopulated due to collisional ionization in a similar envelope shape as the ground $1s^2$ configuration. However, an additional higher-frequency oscillation is observed in the population of this excited state. Similar higher-frequency variations, though at much lower amplitude are observed for the $1s$ H-like population. The same effect can also be seen in Fig. 1 as the average ionization increases in a small steplike shape at the first $\approx$50 fs of the pulse. The following configurations diagram illustrates the most dominant atomic processes.

Figure 4 shows the atomic processes for three configurations only, it is important to note that the atomic model includes many other configurations; we focus here on the most populated configurations and most dominant processes. The excited $1s2p$ configuration is being populated mostly via collisional excitation from the ground state. This has been verified by turning off each of the other possible population channels (e.g., three-body recombination $1s \rightarrow 1s2p$). This configuration is depopulated mostly via laser-induced ionization of the $2p$ electron. The ratio between these two rates determines the temporal population of the configuration. As stated in Sec. II our simulations are done in the tunneling regime. The tunneling frequency is higher than the laser frequency. Since the target is at high density the collisional excitation frequency is also higher than the laser frequency. Therefore, the ratio between the populating and depopulating rates depends on the instantaneous field strength. The collisional excitation rate remains almost constant during a laser cycle. The laser field strength changes at the laser frequency $\approx 10^{15} s^{-1}$. When the field is at its maximum, it quickly depopulates the $1s2p$ configuration. When the field is at its minimum, no depopulation takes place and the fractional population of the $1s2p$ configuration increases.

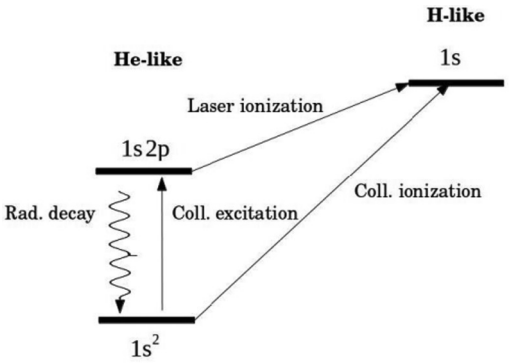

FIG. 4. Configurations diagram for the main atomic processes in the target under the laser field.

V. LASER-INDUCED IONIZATION

Since the $1s2p \rightarrow 1s^2$ is a radiative transition, the atomic kinetics described above will have an imprint on the radiation emitted from the target as well. We now turn to check the effect of the laser-induced ionization process on the radiation emitted from the target during the laser pulse. The $1s2p \rightarrow 1s^2$ transition is at photon energy of 305 eV.

In Fig. 5 the role of the laser-induced ionization is modeled in four ways:

(i) time-dependent ionization rate with no averaging over the laser cycle;

(ii) time-dependent ionization rate only for the pulse envelope but averaged for the laser cycle, using the averaged rate in Ref. [24];

(iii) time-dependent ionization rate only for the pulse envelope; the laser field is taken to be constant during the pulse $E(t) = E_0$;

(iv) no laser-induced ionization is included in the CRM and the laser effect is taken only as a heating source to the target.

In all four treatments, the x-ray pulse envelope is similar. This is due to the transient population of the He-like ionization stage, caused by collisional processes. The $1s2p$ configuration gets quickly populated at the early stages of the laser pulse. The dominant process populating this configuration is the collisional excitation from the He-like ground state. At later times this configuration is not populated as described in Sec. III. At the intermediate time both the ground and the excited configuration are populated. The laser field is not strong enough for ionizing the He-like ground configuration. The excited configuration, however, can be ionized by the laser. the laser-induced ionization of the $1s2p$ configuration will lead to a suppression of the radiation emitted at the 305 eV spectral range, which results from the $1s2p \rightarrow 1s^2$ bound-bound transition. The effect of the laser-induced ionization is best demonstrated in the two extreme cases. When the laser is taken to be a heating source only, no suppression of the x-ray pulse takes place. The laser-induced depopulation of the $1s2p$ configuration is turned off and therefore the simulated signal is maximal. At the other extreme, when the laser field is kept at its maximum value during the interaction, the largest suppression of the signal is achieved. The laser-induced depopulation of the $1s2p$ configuration is at its maximum throughout the pulse. This is in agreement with the minimal values obtained for the full time-dependent simulation. When the laser pulse ends at the time of 100 fs, the laser-induced suppression is shut off and all simulations behave in the same way.

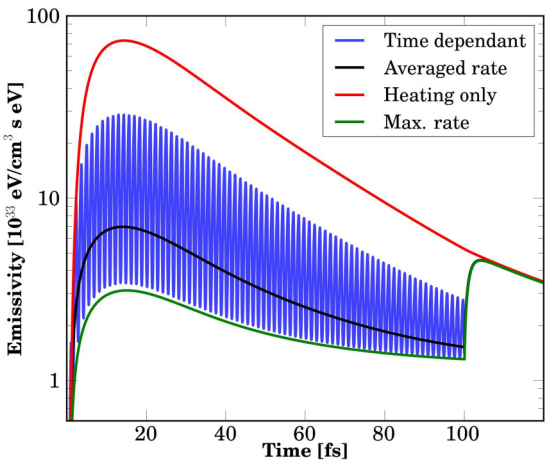

FIG. 5. Radiation emitted at photon energy of 305 eV. the emission is presented for four treatments of the laser induced ionization rate: detailed time-dependent laser ionization oscillating curve (blue); laser ionization averaged for the laser cycle [24] curve (middle, black); laser ionization where the laser field taken to be constant during the pulse $E(t) = E_0$ bottom curve (green); no laser induced ionization, laser effect is taken only as a heating source curve (top, red).

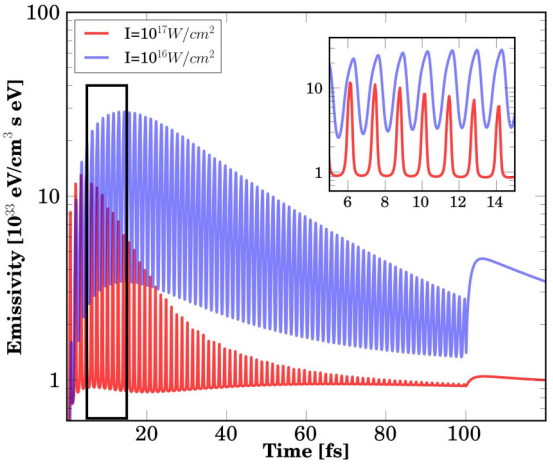

FIG. 6. Radiation emitted at photon energy of 305 eV. For laser intensities of 10^{16}W/cm^2 top curve (blue) and 10^{17}W/cm^2 bottom curve (red). The insert is a zoom in on the rectangle area.

VI. LASER INTENSITY

We now turn to examine the use of higher laser intensities. In Fig. 6 the x-ray emission at 305 eV for laser intensities of 10^{16}W/cm^2 and 10^{17}W/cm^2 from carbon targets are presented.

As expected, the 305 eV, $1s$-$2p$, x-ray pulse envelope for the 10^{17}W/cm^2 laser intensity case decays faster than in the 10^{16}W/cm^2 case. This is due to the faster heating of the target. At a shorter time scale in the zoomed insert, two effects can be observed. First, the duration of peak emission intensity become shorter for the higher-intensity laser. Second, the ratio between the minimum and maximum emission values is larger for the higher-intensity laser. Both of these effects can be understood according to the atomic kinetics described in Sec. IV. At higher laser intensity the laser-induced depopulation of the excited $1s2p$ configuration is strong during a larger part of the laser cycle, therefore allowing for shorter periods of peak population. The depopulation is also more effective at higher intensity leading the larger peak to valley ratio.

VII. AL TARGET

The effect presented in Secs. III–VI is not unique to carbon targets only. Similar phenomena can be found at various low-Z target materials. As an additional example, let us look at the

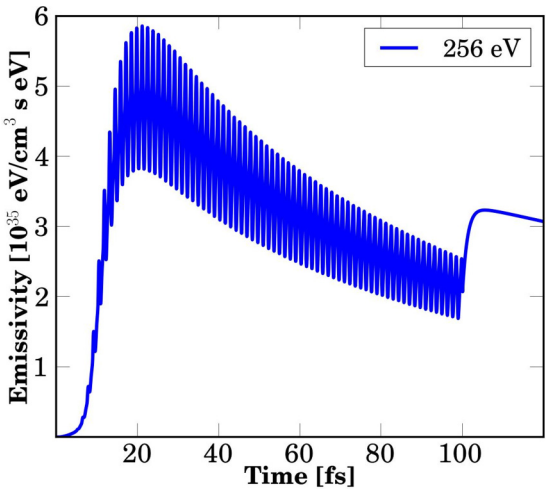

FIG. 7. Radiation emitted at photon energy of 256 eV.

radiation emitted at 256 eV from an aluminum target at natural solid density of $2.7\mathrm{g/cm}^3$. Here again the laser wavelength $\lambda = 0.8\mu\mathrm{m}$. The laser pulse time is taken to be: $\tau_l = 100\,\mathrm{fs}$ and we assume top-hat laser temporal shape for simplicity. The laser intensity is taken to be $I = 10^{16}\mathrm{W/cm}^2$. In this case we look at the Li-like $2s$-$3p$ transition at 256 eV photon energy. The time dependent emission is presented in Fig. 7.

This emission comes from the radiative decay of the $1s^2 3p$ excited configuration, to the ground Li-like configuration $1s^2 2s$. The kinetic picture in this case is similar to the carbon case. The final ionization stage of the target is He-like. The Li-like configurations are, therefore, transient. The laser field is not strong enough to directly ionize the ground configuration Li-like ions. Laser-induced ionization is, however, possible as a two-step process of collisional excitation to the $1s^2 3p$ configuration where the laser can further ionize the $3p$ electron. Due to the high collision rate at the solid target a non-negligible population can be accumulated in the excited state during the laser oscillations, leading to high-frequency oscillating emitted radiation.

The oscillations magnitude in this case is smaller than in the carbon case. This is due to two effects. First, since aluminum has a higher Z number than carbon the ionization potential of the excited $3p$ electron is still larger than in the carbon case. This causes the laser ionization rate of the excited state to be slightly slower in the aluminum case. Second, the electron density in the aluminum case is higher due to the higher density of the target and the higher atomic number. This leads to higher collisional rates.

In order to evaluate the laser intensity needed to cause an oscillating population in a certain excited configuration, for any material, four conditions have to be met. First, the laser ionization rate given by Eq. (15) have to be larger than the laser frequency. This ionization rate depends on the ionization potential of the excited configuration, E_i. Second, the collisional excitation rate from the ground state to the excited state has to be greater than the laser frequency. This rate depends on the energy difference between the ground state and the excited state ΔE. Third, the laser ionization rate has to be much larger than the collisional excitation rate for the laser to depopulate the excited state when at its peak. Fourth, the laser ionization is at the tunneling regime. The collisional excitation rate is proportional to $\exp(-\Delta E/T)$, while the laser ionization rate according to Eq. (15) is proportional to $\exp\left[-2/3(E_i/E_h)^{3/2}E_a/E(t)\right]$. Using these relations one gets the following condition for the laser minimal field strength:

$$E_0 \gg \frac{\frac{2}{3}\left(\frac{E_i}{E_h}\right)^{3/2}T}{\Delta E} \times E_a. \tag{18}$$

One has to find the minimal laser intensity for which all conditions are met. Therefore, Eq. (18) gives a minimum boundary for the laser intensity.

VIII. CONCLUSIONS

In this work the atomic kinetics of solid low-Z materials under intense fs laser pulse have been presented and analyzed. Atomic phenomena on two time scales were identified. First, on the time scale of 20–100 fs the target is heated and collisionally ionized. In this process excited atomic configurations can be temporarily populated. The second phenomena takes place on the time scale of the laser cycle. High-frequency oscillations in the population of some excited configurations have been demonstrated. These oscillations are caused by the competition between two processes, collisional processes populating the excited state and laser-induced ionization depopulating the configuration.

The influence of the oscillating population on the radiation emitted from the target has been demonstrated in Sec. V. The effect of laser intensity was demonstrated in Sec. VI. The higher-intensity laser pulse, resulted in a shorter total emission, due to the faster heating of the target. Moreover, at higher laser intensities the high-frequency oscillations pattern is also changed. The periods of peak emission become shorter as the field-induced ionization is dominant over a larger fraction of the laser cycle.

Finally, the effects of the atomic number and target density were presented in Sec. VII. The kinetic picture demonstrated for carbon was found to be valid for aluminum targets as well. However, since in the Al case both the ionization potential and the electron density are higher, a smaller effect of the oscillating laser field was observed.

The sensitivity of the results presented in the present paper was checked with respect to three parameters. First, the $1/e$ decay factor of the laser intensity within the skin depth. This was found to have a small effect on the emitted radiation form. The most dominant effect of this decay is a small increase in the total emission duration. This increase is caused by deeper layers in the target where the laser field is slightly weaker and therefore these layers emit for a slightly longer duration. It has been verified that this variation in the field strength does not change the transient and oscillating behavior significantly. The second effect that was checked was the laser bandwidth. In all the calculations presented in the present paper the laser was assumed to be purely monochromatic. For a real laser system, some bandwidth of the laser have to be taken into account. For the case of Ti:sapphire laser pulse, the central wavelength is $\lambda = 0.8\mu\mathrm{m}$. A sensitivity check using a laser bandwidth of $\lambda = 0.7$–$0.9\mu\mathrm{m}$ was performed. A temporal broadening of the oscillating x-ray pattern was observed in the simulations. However, for these parameters the oscillations

remain resolvable. Third, the hydrodynamic expansion of the foil in the duration of the laser can lead to a density decrease of up to a factor of two in the skin layer region. It has been verified that this expansion does not change the results presented in this work.

In this work we have focused on the atomic kinetics within the skin layer of the target where the laser field penetrates. This layer is only 10–20 nm thick for the cases presented here. In a realistic scenario, this skin layer is not isolated. Energy is carried from the skin layer by thermal electrons and fast electrons into the target [25,26]. The full analysis of the temperature profile in the target is not the aim of this paper. Reference [26] provides self-similar solutions for the heat wave propagation in the target. It has been verified that the energy loss in the skin layer caused by these processes will not qualitatively change the results presented in this paper. However, the heating of more target material will lead to additional emission in the same spectral ranges. This emission will cause the total pulse to be longer and might mask the oscillations effect. This problem can possibly be eliminated by using a two layers target: a thin layer of low-Z material supported on a higher-Z material. In this way, the emission from the additional heated material will be at different spectral ranges, which can be easily separated. A second effect that needs be considered when designing an experiment to measure this oscillating x-ray emission is the presence of a secondary emission at the same spectral range after the pulse ends. This secondary pulse is a result of the plasma cooling down to temperatures where the relevant excited state becomes populated again. This secondary emission will not have the oscillating nature of the first emission period. In order to estimate the time and duration of this emission, a radiation-hydrodynamic simulation was preformed using the FLORENCE code [27]. It was found that this secondary pulse will carry more energy then the first pulse. The second emission period will begin $\approx$0.3–0.5ps after the first emission.

Another possible application of the phenomena described in the present paper is to experimentally measure the ratio between collisional excitation rates and the laser-induced ionization rate. Three quantities of the emitted radiation depend on this ratio: the x-ray oscillations magnitude, the total amplitude of the pulse and the pulse duration.

In this work we have presented and analyzed the atomic kinetics of solid low-Z materials under intense fs laser pulse field. According to our calculations, this interaction can result in fs to sub-fs x-ray pulses, for the right choice of the experimental parameters: target material, target density, and laser intensity to match the target atomic levels.

[1] M. D. Perry and G. Mourou, Terawatt to petawatt subpicosecond lasers, Science **264**, 917 (1994).

[2] T. Ditmire, T. Donnelly, A. M. Rubenchik, R. W. Falcone, and M. D. Perry, Interaction of intense laser pulses with atomic clusters, Phys. Rev. A **53**, 3379 (1996).

[3] T. Ditmire, Simulations of heating and electron energy distributions in optical field ionized plasmas, Phys. Rev. E **54**, 6735 (1996).

[4] Y. Nagata, K. Midorikawa, S. Kubodera, M. Obara, H. Tashiro, and K. Toyoda, Soft-x-ray Amplification of the Lyman-α Transition by Optical-Field-Induced Ionization, Phys. Rev. Lett. **71**, 3774 (1993).

[5] B. E. Lemoff, G. Y. Yin, C. L. Gordon III, C. P. J. Barty, and S. E. Harris, Demonstration of a 10-Hz Femtosecond-Pulse-Driven Xuv Laser at 41.8 nm in Xe Ix, Phys. Rev. Lett. **74**, 1574 (1995).

[6] J. D. Kmetec, C. L. Gordon, III, J. J. Macklin, B. E. Lemoff, G. S. Brown, and S. E. Harris, Mev X-ray Generation with a Femtosecond Laser, Phys. Rev. Lett. **68**, 1527 (1992).

[7] A. Zigler, T. Palchan, N. Bruner, E. Schleifer, S. Eisenmann, M. Botton, Z. Henis, S. A. Pikuz, A. Y. Faenov Jr, D. Gordon *et al.*, 5.5–7.5 MeV Proton Generation by a Moderate-Intensity Ultrashort-pulse Laser Interaction with H_2O Nanowire Targets, Phys. Rev. Lett. **106**, 134801 (2011).

[8] A. Zigler, S. Eisenman, M. Botton, E. Nahum, E. Schleifer, A. Baspaly, I. Pomerantz, F. Abicht, J. Branzel, G. Priebe *et al.*, Enhanced Proton Acceleration by an Ultrashort Laser Interaction with Structured Dynamic Plasma Targets, Phys. Rev. Lett. **110**, 215004 (2013).

[9] A. Zewail, Laser femtochemistry, Science **242**, 1645 (1988).

[10] M. M. Murnane, H. C. Kapteyn, M. D. Rosen, and R. W. Falcone, Ultrafast x-ray pulses from laser-produced plasmas, Science **251**, 531 (1991).

[11] N. Zhang, X. Zhu, J. Yang, X. Wang, and M. Wang, Time-Resolved Shadowgraphs of Material Ejection in Intense Femtosecond Laser Ablation of Aluminum, Phys. Rev. Lett. **99**, 167602 (2007).

[12] J. D. Huba, Nrl: Plasma formulary, Technical report, DTIC Document (2004).

[13] S. Eliezer, *The Interaction of High-Power Lasers with Plasmas* (CRC Press, Boca Raton, 2002).

[14] H. M. Milchberg, R. R. Freeman, S. C. Davey, and R. M. More, Resistivity of a Simple Metal from Room Temperature to 10^6 K, Phys. Rev. Lett. **61**, 2364 (1988).

[15] P. Sprangle, J. Peñano, B. Hafizi, D. Gordon, and M. Scully, Remotely induced atmospheric lasing, Appl. Phys. Lett. **98**, 211102 (2011).

[16] M. Born and E. Wolf, *Principles of Optics: Electromagnetic Theory of Propagation, Interference and Diffraction of Light* (Cambridge University Press, Cambridge, 1999).

[17] A. Bar-Shalom, M. Klapisch, and J. Oreg, Hullac, an integrated computer package for atomic processes in plasmas, J. Quant. Spectrosc. Radiat. Transfer **71**, 169 (2001), Radiative Properties of Hot Dense Matter.

[18] Y. Frank, E. Louzon, P. Mandelbaum, and Z. Henis, Semillac: A new hybrid atomic model of hot dense plasmas, High Energy Density Phys. **9**, 594 (2013).

[19] Y. Frank, P. Mandelbaum, and Z. Henis, Semillac ii: A new model for spectral behavior of hot plasmas, High Energy Density Phys. **12**, 27 (2014).

[20] J. C. Stewart and K. D. Pyatt Jr, Lowering of ionization potentials in plasmas, Astrophys. J. **144**, 1203 (1966).

[21] L. D. Landau and E. M. Lifshitz, *Quantum Mechanics*, 3rd ed. (Pergamon, London, 1978).

[22] L. V. Keldysh, Ionization in the field of a strong electromagnetic wave, Sov. Phys. JETP **20**, 1307 (1965).

[23] U. Mohideen, M. H. Sher, H. W. K. Tom, G. D. Aumiller, I. I. O. R. Wood, R. R. Freeman, J. Boker, and P. H. Bucksbaum, High Intensity above-Threshold Ionization of He, Phys. Rev. Lett. **71**, 509 (1993).

[24] P. B. Corkum, N. H. Burnett, and F. Brunel, Above-threshold ionization in the long-wavelength limit, Phys. Rev. Lett. **62**, 1259 (1989).

[25] P. Gibbon, Efficient Production of fast Electrons from Femtosecond Laser Interaction with Solid Targets, Phys. Rev. Lett. **73**, 664 (1994).

[26] W. Rozmus and V. T. Tikhonchuk, Skin effect and interaction of short laser pulses with dense plasmas, Phys. Rev. A **42**, 7401 (1990).

[27] Y. Frank, E. Raicher, Y. Erlich, G. Hurvitz, Z. Shpilman, M. Fraenkel, A. Zigler, and Z. Henis, Influence of atomic modeling on integrated simulations of laser-produced au plasmas, Phys. Rev. E **92**, 053111 (2015).